

Semiconductor-based selective emitter with sharp cutoff for thermophotovoltaic energy conversion

QING NI*, RAJAGOPALAN RAMESH, CHENG-AN CHEN, LIPING WANG*

School for Engineering of Matter, Transport & Energy, Arizona State University, Tempe, Arizona, 85287, USA

*Corresponding author: qingni@asu.edu (Q.N.); liping.wang@asu.edu (L.W.)

Received XX Month XXXX; revised XX Month, XXXX; accepted XX Month XXXX; posted XX Month XXXX (Doc. ID XXXXX); published XX Month XXXX

Semiconductor emitter can possibly achieve sharp cutoff wavelength due to its intrinsic bandgap absorption and almost zero sub-bandgap emission without doping. A germanium wafer based selective emitter with front-side antireflection and backside metal coating is studied here for thermophotovoltaic (TPV) energy conversion. Optical simulation predicts the spectral emittance above 0.9 in the wavelengths from 1 to 1.85 μm and below 0.2 in the sub-bandgap range with sharp cutoff around the bandgap, indicating superior spectral selectivity behavior. This is confirmed by excellent agreement with indirectly measured spectral emittance of the fabricated Ge-based selective emitter sample. Furthermore, the TPV efficiency by paring the Ge-based selective emitter with a GaSb cell is theoretically analyzed at different temperatures. This work will facilitate the development of the semiconductor-based selective emitters for enhancing TPV performance.

Thermophotovoltaic (TPV) devices convert thermal radiation from a high-temperature emitter to electricity via a narrow-bandgap photovoltaic (PV) cell. Since the emitter can be heated by any kind of heat source (combustible fuel, solar energy, waste heat, etc.), TPV technique has a wide range of applications. The theoretical efficiency of the TPV system has the Carnot limit [1]. However, due to the mismatch between the thermal radiation spectrum of the emitter and the absorption spectrum of the cell, the practical TPV system has low output electric power and poor efficiency [2-4]. To overcome this problem, much work has been carried out on spectrally selective emitters that emit photons with energy just above the bandgap of the PV cell. An ideal selective emitter should have an emissivity of one over a certain bandwidth just above the bandgap of the PV cell, and an emissivity of zero elsewhere. In addition, spectrally selective PV cells have also recently been demonstrated to enhance TPV efficiency exceeding 30% at 1455 K by recycling the unused photons to the emitter [5].

Previous works have demonstrated that the spectrally selective emitters can be achieved and tuned by photonic crystals [6-8] and metamaterials [9-12] structures. However, the complex geometries and the difficulty of fabrication process prevents the low-cost fabrication. High temperature stability after long-term practical operation with these nanostructures is another big concern. Spectrally selective emitters can also be realized by multilayer structures based on the anti-reflection effect or cavity resonance [4, 13, 14], which are much easier to fabricate potentially at large scale. Based on Kirchhoff's law of thermal radiation [15] that absorptivity equals emissivity at every wavelength in thermal equilibrium, spectrally selective absorbers may also serve as spectrally selective emitters. Wang et al. [13] previously reported a multilayer selective solar absorber which has good spectral selectivity behavior and high temperature stability. However, the cutoff wavelength, i.e.,

the transition between the high emittance above the bandgap and the low emittance below the bandgap, is not sharp, still resulting in some undesirable photons below the bandgap.

There is a less-studied category in semiconductor-based selective emitter, which has the potential for ideal emitter since the semiconductor bandgap edge itself provides a natural sharp cutoff wavelength. Previous works have theoretically designed semiconductor-metal tandem structures using Si and Ge mainly for solar thermal absorption [16, 17]. Tian et al. [18] experimentally demonstrated a low-cost single-crystal Si wafer based selective absorber with Si_3N_4 anti-reflective (AR) coating. Zhou et al. [19] fabricated a 9.6- μm thin-film Si based selective emitter with good mechanical flexibility and thermal stability at 600°C, and demonstrated strongly suppresses thermal emittance in the mid-IR over thicker silicon wafers. In addition, Oh et al. [20] proposed a selective emitter with a single layer of cylindrical structure of p-type silicon, which has a absorption peak in mid-IR range for TPV application. While most of the previous works on semiconductor-based selective absorber/emitter focused on Si, Ge which has a lower energy bandgap (0.67 eV) should be more suitable for TPV application.

In this work, we investigate a semiconductor-based selective TPV emitter made of a 500- μm -thick undoped Ge wafer with a 150-nm-thick Si_3N_4 front layer and a 200-nm-thick tungsten layer on the backside. The Si_3N_4 layer acts as an AR coating to reduce in-band reflection thus enhancing absorption or emission, while the tungsten layer is used to ensure the opaqueness of the structure with high reflectivity below the bandgap of Ge. In order to predict the spectral directional emittance, the indirect method is used here by calculating the spectral directional reflectance of the proposed structure. According to Kirchhoff's law, the spectral directional emittance is equal to the spectral

directional absorptance as $1 - R'_\lambda$ from energy balance with zero transmittance due to the opaque backside tungsten film. As illustrated in Fig. 1(a), ρ_a or ρ_b respectively represent the reflectivity of the Si_3N_4 thin layer for rays originated from air or from the Ge substrate, whereas τ_a or τ_b are the corresponding transmissivity. ρ_s represents the reflectivity of the tungsten layer for rays originated from the Ge substrate. All above spectral directional reflectivity and transmissivity are calculated with the thin-film optics method [21, 22] for the Si_3N_4 front layer and the tungsten back coating separately. The light propagation inside the incoherent thick Ge substrate is taken into consideration by the ray-tracing method, and consequently, the spectral directional reflectance of the proposed Ge-based selective emitter with front and backside coatings can be calculated as [22]:

$$R'_\lambda = \rho_a + \rho_s \tau_a^2 \tau^2 / (1 - \rho_s \rho_b \tau^2) \quad (1)$$

where $\tau = \exp(-4\pi\kappa_s d_s / \lambda \cos\theta_s)$ is the internal transmissivity of the Ge substrate with extinction coefficient κ_s , thickness d_s , free-space wavelength λ , and refraction angle θ_s inside the Ge substrate calculated from incident angle θ_1 with Snell's law.

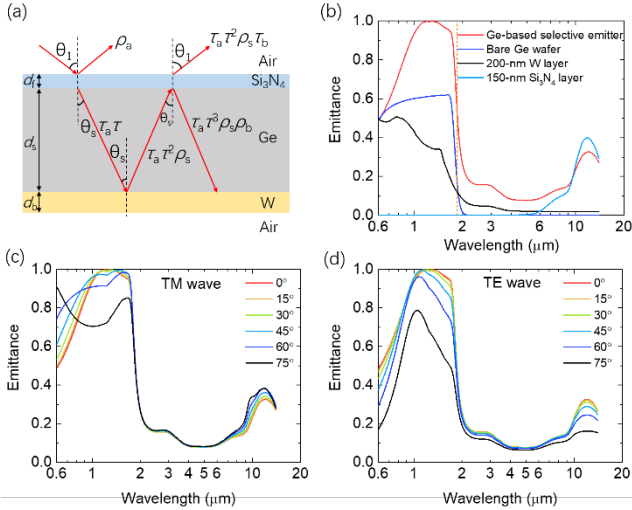


Fig. 1. (a) Schematic of the proposed Ge-based emitter structure and the wave propagation. (b) Theoretical normal spectral emittance of the proposed Ge-based emitter. Theoretical spectral emittance of the proposed Ge-based emitter at different incident angles for (c) TM wave and (d) TE wave.

Fig. 1 (b) shows the theoretical spectral emittance of the proposed Ge-based selective emitter. In the calculation, the optical constant of Si_3N_4 and tungsten are from Palik data [23], while the optical constants of undoped Ge are from Ref. [24]. For comparison, the simulated emittance spectra of a 150-nm Si_3N_4 layer, 200-nm tungsten film, and 500- μm bare undoped Ge wafer, were also shown in the figure where the dash line represents the Ge bandgap at 1.85 μm wavelength (i.e., 0.67 eV). As expected, undoped Ge has almost zero sub-bandgap emission with around 0.6 in-band emittance due to bandgap absorption. With the Si_3N_4 antireflection coating, the in-band emittance of the Ge-based selective emitter is significantly enhanced, reaching unity at wavelength of 1.3 μm right above the bandgap. Right below the bandgap, the emittance sharply drops to 0.1

or so due to the absorption of the lossy tungsten layer. At longer wavelengths beyond 10 μm , the emittance increases up to 0.3 or so because of strong phonon absorption of Si_3N_4 . Fig. 1(c) and 1(d) respectively present the spectral emittance at different angles for transverse-magnetic (TM) and -electric (TE) polarized waves. It can be seen that at the wavelength below the bandgap, the emittance slightly increases with the incident angle for TM waves at first and then decreases at large incident angle, which is due to the Brewster effect [22, 25]. For non- or lightly absorbing materials, reflectance at TM waves could decrease to minimum at a particular incidence angle, namely Brewster angle. For the undoped Ge wafer used in this work, the Brewster angle is about 75° calculated by $\theta = \tan^{-1}(n_2/n_1)$ [22], where n_2 and n_1 represent the refractive index of Ge and air, respectively. Therefore, the reflectance at TM waves should decrease with incident angle from 0° to 75° , which explains the trend of emittance shown in Fig. 1(c). While for TE waves, the emittance decreases monotonically with the incident angle, which means the reflectance increases monotonically with the incident angle. Overall, the spectral emittance of the proposed structure is insensitive to the incident angles at small incident angles, indicating that the Ge-based selective emitter has diffuse emission behavior.

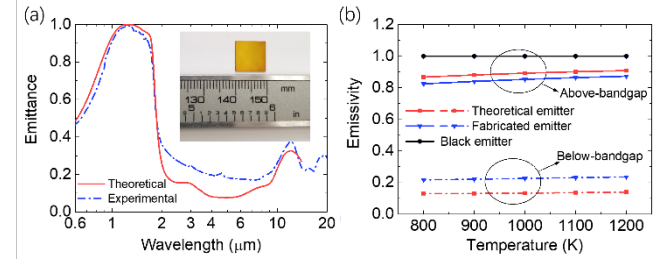


Fig. 2. (a) Spectral emittance of the fabricated Ge-based selective emitter sample. Inset is the photo of the fabricated Ge-based selective emitter on the Si_3N_4 side. (b) Spectrally averaged efficiency at different temperatures.

To experimentally demonstrate that the proposed structure has a good spectral selectivity, a Ge-based selective emitter sample was fabricated on a 500- μm -thick (100) double-sided polished Ge wafer (50 $\Omega\cdot\text{cm}$, MTI Corporation) with the size of $1 \times 1 \text{ cm}^2$. Before the deposition of films, the Ge wafer was plasma cleaned. A 200-nm tungsten layer was firstly sputtered (Lesker PVD75 Sputter Coater) on one side of the Ge wafer at a rate of 1 \AA/s under vacuum pressure of 1×10^{-6} Torr. Then a 150-nm Si_3N_4 layer was deposited on the other side of the Ge wafer using Plasma-enhanced chemical vapor deposition (PECVD) method (Oxford Plasmalab100) at a rate of 290 \AA/min under the temperature of 300°C . The root-mean-square surface roughness of the fabricated sample was found to be around 0.9 nm with atom force microscope.

The spectral normal reflectance of the fabricated sample was characterized by Fourier-transform spectroscopy (Thermo Fisher Scientific, Nicolet iS50) along with a specular reflection accessory (Harrick Scientific, Seagull) at an incidence angle of 8° in wavelength from 0.4 to 20 μm with a resolution of 4 cm^{-1} in wavenumber. The spectral reflectance from 0.4 to 1 μm was measured by a Si detector, while that beyond 1 μm was measured by a deuterated triglycine sulfate (DTGS) detector. An aluminum mirror was

used as the reference and the measured results was corrected by the theoretical reflectance of aluminum with optical constants obtained from Palik [23]. Each spectrum was averaged over 32 scans, and three independent measurements for both Al mirror and the sample were taken for consistency. The spectral normal emittance of the sample can be obtained by one minus spectral normal reflectance, as shown in Fig. 2(a). Inset is the photo of the fabricated sample. It can be observed that the measured spectral emittance of the fabricated sample agrees well with the simulated one above the bandgap. Below the bandgap the measured result is around 5% higher than the theoretical one, probably caused by the higher loss of the sputtered tungsten film due to grains and slightly oxidation that leads to different optical constants of tungsten from Palik.

To evaluate the spectral selectivity of the proposed emitter, we calculated the spectrally averaged emittance for above-bandgap spectrum $\bar{\varepsilon}_{\text{above}}$ and below-bandgap spectrum $\bar{\varepsilon}_{\text{below}}$ as:

$$\bar{\varepsilon}_{\text{above}} = \int_0^{\lambda_{\text{gc}}} \varepsilon_{\lambda} E_{b,\lambda}(T) d\lambda / \int_0^{\lambda_{\text{gc}}} E_{b,\lambda}(T) d\lambda \quad (2)$$

$$\bar{\varepsilon}_{\text{below}} = \int_{\lambda_{\text{gc}}}^{\infty} \varepsilon_{\lambda} E_{b,\lambda}(T) d\lambda / \int_{\lambda_{\text{gc}}}^{\infty} E_{b,\lambda}(T) d\lambda \quad (3)$$

where $\lambda_{\text{gc}} = 1.85 \mu\text{m}$ is the bandgap wavelength of Ge, $E_{b,\lambda}(T) = 2\pi hc_0^2 / \lambda^5 [\exp(hc_0 / \lambda k_B T) - 1]$ is the blackbody spectral emissive power [15] with Planck's constant h , the speed of light in vacuum c_0 , Boltzmann constant k_B , and absolute temperature T . Fig. 2 (b) show $\bar{\varepsilon}_{\text{above}}$ and $\bar{\varepsilon}_{\text{below}}$ at different temperatures for both theoretical Ge-based selective emitter and fabricated sample. It can be seen that both $\bar{\varepsilon}_{\text{above}}$ and $\bar{\varepsilon}_{\text{below}}$ of the theoretical Ge-based selective emitter barely change with the temperature between 800 and 1200 K. The same trend is shown for the fabricated sample. For the theoretical Ge-based selective emitter, the above-bandgap averaged emittance $\bar{\varepsilon}_{\text{above}}$ is 0.91 while the below-bandgap averaged emittance $\bar{\varepsilon}_{\text{below}}$ is 0.14 at 1200 K. In comparison, the black emitter has the emittance of 1 for the whole spectrum. Therefore, the proposed Ge-based selective emitter demonstrates good spectral selectivity.

The spectral efficiency can be defined as the percentage of the photons from the emitter absorbed by the PV cell:

$$\eta_{\text{spectral}} = \int_0^{\lambda_{\text{gc}}} q_{e-c,\lambda} d\lambda / \int_0^{\infty} q_{e-c,\lambda} d\lambda \quad (4)$$

where λ_{gc} is the bandgap wavelength of the PV cell,

$$q_{e-c,\lambda} = \frac{E_{be,\lambda}(T_e) - E_{bc,\lambda}(T_c)}{1/\varepsilon_{e,\lambda} + 1/\varepsilon_{c,\lambda} - 1}$$

is the spectral net radiative heat flux between the emitter and the cell with a view factor of 1, and the subscript e(c) represents the emitter (cell). $\varepsilon_{e,\lambda}$ is the spectral emissivity of the emitter and $\varepsilon_{c,\lambda}$ is the spectral emittance (or absorptance) of the PV cell, both of which are assumed diffuse. T_e and T_c are respectively the emitter temperature and the cell temperature. GaSb cell with a close-to-Ge bandgap of 0.72 eV, which can be fabricated using molecular beam epitaxial and Zn diffusion methods to form

p-n junction [26], is used here for the TPV modeling. T_c is assumed to be 300 K in this work. Note that the in-band spectral absorptance of GaSb cell is obtained from Ref [26], and out-of-band absorptance is taken as 0.5 as a nominal value. Fig. 3(a) shows the spectral efficiency of the theoretical Ge-based selective emitter at different temperatures. For comparison, the spectral efficiencies of the fabricated sample and a black emitter ($\varepsilon_{e,\lambda}=1$) are also shown. The spectral efficiency will increase with the emitter temperature, which is because that the thermal radiation spectrum shifts to lower wavelength as the temperature increases, thus increasing the percentage of the photons with energies above the bandgap of the PV cell. Note that the theoretical Ge-based selective emitter has higher spectral efficiency than the fabricated sample due to its lower sub-bandgap emittance. The proposed Ge-based selective emitter has higher spectral efficiency than a black emitter. At a temperature of 1200 K, the spectral efficiency of the theoretical Ge-based selective emitter can achieve 34.0%, while that of a black emitter is only 12.0%.

To discuss the performance with the proposed Ge-based selective emitter, the TPV efficiency η can be calculated by

$$\eta = P_e / q_{\text{in}} \quad (5)$$

where $P_e = J_{\text{sc}} V_{\text{oc}} FF$ is the maximum output electric power

density produced by the PV cell. $J_{\text{sc}} = \int_0^{\lambda_{\text{gc}}} \frac{e\lambda}{hc_0} \eta_{\text{IQE},\lambda} q_{e-c,\lambda} d\lambda$

(A/cm²) is the short-circuit current density [27]. Note that E_g is the bandgap of the PV cell, e is an elementary charge, and $\eta_{\text{IQE},\lambda}$ is the internal quantum efficiency (IQE) of the PV cell. $V_{\text{oc}} = (k_B T_c / e) \ln(J_{\text{sc}} / J_0 + 1)$ is the open-circuit voltage (V) [27], in which J_0 is the dark current calculated by $J_0 = e [n_i^2 D_h / (L_h N_D) + n_i^2 D_e / (L_e N_A)]$. n_i is the intrinsic carrier concentration of the semiconductor, N_D and N_A are respectively the donor concentration and acceptor concentration, D_h and D_e are respectively the hole diffusion coefficient and electron diffusion coefficient, and L_h and L_e are respectively the hole and electron diffusion length. FF is the filling factor calculated by $FF = (1 - 1/y)(1 - \ln y / y)$, in which $y = \ln(J_{\text{sc}} / J_0)$. All the calculation parameters of the

GaSb cell are taken from Ref. [26]. $q_{\text{in}} = \int_0^{\infty} q_{e-c,\lambda} d\lambda$ is the net radiative heat flux between the emitter and the cell with the same area.

Fig. 3(b), (c) and (d) respectively predict the TPV efficiency, the net radiative heat flux between the emitter and the PV cell, and the output power for the TPV system using the Ge-based selective emitter paired with a GaSb cell. For comparison, the results using a black emitter are also shown. With a black emitter at temperature from 800 to 1200 K, the TPV efficiency ranges from 0.3% to 4.0%. While with the fabricated Ge-based selective emitter sample, the TPV efficiency was improved ranging from 0.8% to 8.2%, which is due to the good spectral selectivity of the Ge-based selective emitter with low emittance below the bandgap, thus reducing the net radiative heat flux with almost the same power output. With a theoretical Ge-based selective

emitter, the TPV efficiency could be further improved ranging from 1.2% to 11.2%, which is due to its lower sub-bandgap emittance, thus further reducing the net radiative heat flux. Note that these three emitters produce similar P_e below 1000 K. As the emitter temperature increases, the black emitter will surpass the proposed Ge-based selective emitter. P_e depends on the net radiative heat flux above the bandgap of the cell. At low temperature, the emissive power from the emitter at short wavelength (above the bandgap) is low, which causes similar power from these three emitters. As the temperature increases, the thermal emission spectrum shifts to shorter wavelength. The black emitter has the highest emittance, resulting in the highest net radiative heat flux above the bandgap, thus producing the highest output power. While the fabricated Ge-based selective emitter sample has the lowest emittance, resulting in the lowest net radiative heat flux above the bandgap, thus producing the lowest power. In particular, at an emitter temperature of 1200 K, the theoretical Ge-based selective emitter can achieve a TPV efficiency of 11.2% and an output power of 2.3 kW/m².

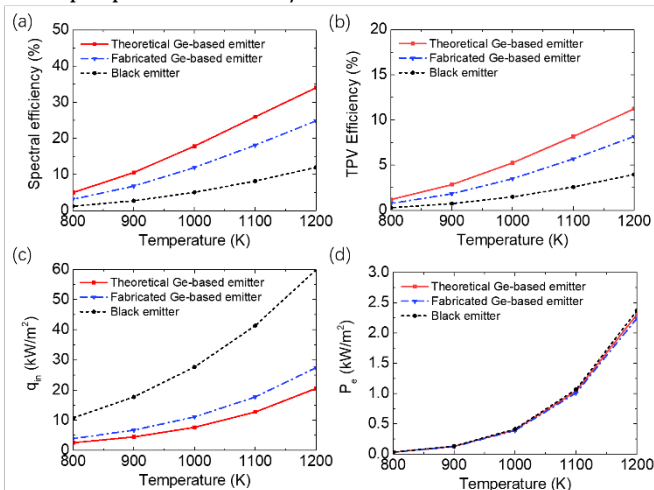


Fig. 3. (a) Spectral efficiency, (b) TPV efficiency, (c) net radiative heat flux and (d) output power at different temperatures from 800 K to 1200 K with theoretical Ge-based emitter, fabricated Ge-based emitter and black emitter paired with a GaSb cell.

In summary, a Ge wafer based selective emitter was proposed for thermophotovoltaic energy conversion. The optical property simulation of the proposed structure demonstrated a good spectral selectivity behavior. We also fabricated the Ge-based selective emitter sample and characterized its spectral emittance, which confirms the theoretical result. Moreover, the TPV system performance was simulated by using the proposed Ge-based selective emitter paired with a GaSb cell. The simulated results show a TPV efficiency of 11.2% and an output power of 2.3 kW/m² at 1200 K. This work will pave the way for the semiconductor-based spectrally selective emitter and will promote the development of the low-cost and high-efficiency TPV devices.

Funding. National Science Foundation (CBET-1454698); Air Force Office of Scientific Research (FA9550-17-1-0080).

Acknowledgments. We would like to thank Dr. Linshuang Long for taking the surface roughness measurement with AFM.

Data Availability. The data that support the findings of this study are available from the corresponding author upon reasonable request.

Disclosures. The authors declare no conflicts of interest.

References

1. A. Karalis and J. Joannopoulos, *Scientific Reports* **6**, 28472 (2016).
2. A. Gombert, *AIP conference proceedings* **653**, 123-131 (2003).
3. A. Datas and A. Martí, *Solar Energy Materials and Solar Cells* **161**, 285-296 (2017).
4. N. A. Pfister and T. E. Vandervelde, *physica status solidi (a)* **214**, 1600410 (2016).
5. D. Fan, T. Burger, S. McSherry, B. Lee, A. Lenert, and S. R. Forrest, *Nature* **586**, 237-241 (2020).
6. A. Lenert, D. M. Bierman, Y. Nam, W. R. Chan, I. Celanović, M. Soljačić, and E. N. Wang, *Nature nanotechnology* **9**, 126-130 (2014).
7. Y. Nam, Y. X. Yeng, A. Lenert, P. Bermel, I. Celanovic, M. Soljačić, and E. N. Wang, *Solar Energy Materials and Solar Cells* **122**, 287-296 (2014).
8. J. H. Kim, S. M. Jung, and M. W. Shin, *Optical Materials* **72**, 45-51 (2017).
9. D. N. Woolf, E. A. Kadlec, D. Bethke, A. D. Grine, J. J. Nogan, J. G. Cederberg, D. B. Burckel, T. S. Luk, E. A. Shaner, and J. M. Hensley, *Optica* **5**, 213-218 (2018).
10. D. M. Bierman, A. Lenert, W. R. Chan, B. Bhatia, I. Celanović, M. Soljačić, and E. N. Wang, *Nature Energy* **1**, 16068 (2016).
11. H. Wang, J.-Y. Chang, Y. Yang, and L. Wang, *International Journal of Heat and Mass Transfer* **98**, 788-798 (2016).
12. M. Chen, X. Chen, H. Yan, and P. Zhou, *Physica E: Low-dimensional Systems and Nanostructures* **126**, 114471 (2021).
13. H. Wang, H. Alshehri, H. Su, and L. Wang, *Solar Energy Materials and Solar Cells* **174**, 445-452 (2018).
14. A. Soum-Glaude, A. Le Gal, M. Bichotte, C. Escape, and L. Dubost, *Solar Energy Materials and Solar Cells* **170**, 254-262 (2017).
15. T. L. Bergman, F. P. Incropera, D. P. DeWitt, and A. S. Lavine, *Fundamentals of heat and mass transfer*, 7 ed. (John Wiley & Sons, 2011).
16. P. Bermel, M. Ghebrebrhan, W. Chan, Y. X. Yeng, M. Araghchini, R. Hamam, C. H. Marton, K. F. Jensen, M. Soljačić, and J. D. Joannopoulos, *Optics express* **18**, A314-A334 (2010).
17. A. Donnadieu and B. Seraphin, *JOSA* **68**, 292-297 (1978).
18. H. Tian, Z. Zhou, T. Liu, C. Karina, U. Guler, V. Shalaev, and P. Bermel, *Applied Physics Letters* **110**, 141101 (2017).
19. Z. Zhou, H. Tian, T. M. Hymel, H. Reddy, V. M. Shalaev, Y. Cui, and P. Bermel, *Optical Materials Express* **10**, 208-221 (2020).
20. M. Oh, E. Carlson, and T. E. Vandervelde, *Journal of Electronic Materials*, 1-8 (2020).
21. L. Wang, S. Basu, and Z. Zhang, *Journal of heat transfer* **133**(2011).
22. Z. M. Zhang, *Nano/microscale heat transfer* (2007).
23. E. D. Palik, *Handbook of optical constants of solids* (Academic press, 1998), Vol. 3.
24. T. N. Nunley, N. S. Fernando, N. Samarasingha, J. M. Moya, C. M. Nelson, A. A. Medina, and S. Zollner, *Journal of Vacuum Science & Technology B, Nanotechnology and Microelectronics: Materials, Processing, Measurement, and Phenomena* **34**, 061205 (2016).
25. R. Ramesh, S. Niauzorau, Q. Ni, B. P. Azeredo, and L. Wang, *Nanotechnology* **31**, 405706 (2020).
26. L. Tang, H. Ye, and J. Xu, *Solar energy materials and solar cells* **122**, 94-98 (2014).
27. K. Park, S. Basu, W. P. King, and Z. Zhang, *Journal of Quantitative Spectroscopy and Radiative Transfer* **109**, 305-316 (2008).

Full Reference List

1. A. Karalis and J. Joannopoulos, "'Squeezing' near-field thermal emission for ultra-efficient high-power thermophotovoltaic conversion," *Scientific Reports* 6, 28472 (2016).
2. A. Gombert, "An overview of TPV emitter technologies," AIP conference proceedings 653, 123-131 (2003).
3. A. Datas and A. Martí, "Thermophotovoltaic energy in space applications: Review and future potential," *Solar Energy Materials and Solar Cells* 161, 285-296 (2017).
4. N. A. Pfister and T. E. Vandervelde, "Selective emitters for thermophotovoltaic applications," *physica status solidi (a)* 214, 1600410 (2016).
5. D. Fan, T. Burger, S. McSherry, B. Lee, A. Lenert, and S. R. Forrest, "Near-perfect photon utilization in an air-bridge thermophotovoltaic cell," *Nature* 586, 237-241 (2020).
6. A. Lenert, D. M. Bierman, Y. Nam, W. R. Chan, I. Celanović, M. Soljačić, and E. N. Wang, "A nanophotonic solar thermophotovoltaic device," *Nature nanotechnology* 9, 126-130 (2014).
7. Y. Nam, Y. X. Yeng, A. Lenert, P. Bermel, I. Celanovic, M. Soljačić, and E. N. Wang, "Solar thermophotovoltaic energy conversion systems with two-dimensional tantalum photonic crystal absorbers and emitters," *Solar Energy Materials and Solar Cells* 122, 287-296 (2014).
8. J. H. Kim, S. M. Jung, and M. W. Shin, "High-temperature degradation of one-dimensional metalodielectric (W/SiO₂) photonic crystal as selective thermal emitter for thermophotovoltaic system," *Optical Materials* 72, 45-51 (2017).
9. D. N. Woolf, E. A. Kadlec, D. Bethke, A. D. Grine, J. J. Nogan, J. G. Cederberg, D. B. Burckel, T. S. Luk, E. A. Shaner, and J. M. Hensley, "High-efficiency thermophotovoltaic energy conversion enabled by a metamaterial selective emitter," *Optica* 5, 213-218 (2018).
10. D. M. Bierman, A. Lenert, W. R. Chan, B. Bhatia, I. Celanović, M. Soljačić, and E. N. Wang, "Enhanced photovoltaic energy conversion using thermally based spectral shaping," *Nature Energy* 1, 16068 (2016).
11. H. Wang, J.-Y. Chang, Y. Yang, and L. Wang, "Performance analysis of solar thermophotovoltaic conversion enhanced by selective metamaterial absorbers and emitters," *International Journal of Heat and Mass Transfer* 98, 788-798 (2016).
12. M. Chen, X. Chen, H. Yan, and P. Zhou, "Theoretical design of nanoparticle-based spectrally emitter for thermophotovoltaic applications," *Physica E: Low-dimensional Systems and Nanostructures* 126, 114471 (2021).
13. H. Wang, H. Alshehri, H. Su, and L. Wang, "Design, fabrication and optical characterizations of large-area lithography-free ultrathin multilayer selective solar coatings with excellent thermal stability in air," *Solar Energy Materials and Solar Cells* 174, 445-452 (2018).
14. A. Soum-Glaude, A. Le Gal, M. Bichotte, C. Escape, and L. Dubost, "Optical characterization of TiAlN_x/TiAlNy/Al₂O₃ tandem solar selective absorber coatings," *Solar Energy Materials and Solar Cells* 170, 254-262 (2017).
15. T. L. Bergman, F. P. Incropera, D. P. DeWitt, and A. S. Lavine, *Fundamentals of heat and mass transfer*, 7 ed. (John Wiley & Sons, 2011).
16. P. Bermel, M. Ghebrebrhan, W. Chan, Y. X. Yeng, M. Araghchini, R. Hamam, C. H. Marton, K. F. Jensen, M. Soljačić, and J. D. Joannopoulos, "Design and global optimization of high-efficiency thermophotovoltaic systems," *Optics express* 18, A314-A334 (2010).
17. A. Donnadieu and B. Seraphin, "Optical performance of absorber-reflector combinations for photothermal solar energy conversion," *JOSA* 68, 292-297 (1978).
18. H. Tian, Z. Zhou, T. Liu, C. Karina, U. Guler, V. Shalaev, and P. Bermel, "High temperature efficient, stable Si wafer-based selective solar absorbers," *Applied Physics Letters* 110, 141101 (2017).
19. Z. Zhou, H. Tian, T. M. Hymel, H. Reddy, V. M. Shalaev, Y. Cui, and P. Bermel, "High-temperature, spectrally-selective, scalable, and flexible thin-film Si absorber and emitter," *Optical Materials Express* 10, 208-221 (2020).
20. M. Oh, E. Carlson, and T. E. Vandervelde, "Design of an All-Semiconductor Selective Metamaterial Emitter in the Mid-IR Regime with Larger Feature Sizes for Thermophotovoltaic Energy Conversion Applications," *Journal of Electronic Materials*, 1-8 (2020).
21. L. Wang, S. Basu, and Z. Zhang, "Direct and indirect methods for calculating thermal emission from layered structures with nonuniform temperatures," *Journal of heat transfer* 133(2011).
22. Z. M. Zhang, *Nano/microscale heat transfer* (2007).
23. E. D. Palik, *Handbook of optical constants of solids* (Academic press, 1998), Vol. 3.
24. T. N. Nunley, N. S. Fernando, N. Samarasingha, J. M. Moya, C. M. Nelson, A. A. Medina, and S. Zollner, "Optical constants of germanium and thermally grown germanium dioxide from 0.5 to 6.6 eV via a multisample ellipsometry investigation," *Journal of Vacuum Science & Technology B, Nanotechnology and Microelectronics: Materials, Processing, Measurement, and Phenomena* 34, 061205 (2016).
25. R. Ramesh, S. Niazorau, Q. Ni, B. P. Azeredo, and L. Wang, "Optical characterization and modeling of nanoporous gold absorbers fabricated by thin-film dealloying," *Nanotechnology* 31, 405706 (2020).
26. L. Tang, H. Ye, and J. Xu, "A novel zinc diffusion process for the fabrication of high-performance GaSb thermophotovoltaic cells," *Solar energy materials and solar cells* 122, 94-98 (2014).
27. K. Park, S. Basu, W. P. King, and Z. Zhang, "Performance analysis of near-field thermophotovoltaic devices considering absorption distribution," *Journal of Quantitative Spectroscopy and Radiative Transfer* 109, 305-316 (2008).